

LARGE EDDY SIMULATION OF VARIABLE DENSITY TURBULENT AXISYMMETRIC JETS

Ping Wang

Institute for Hydromechanics, University of Karlsruhe
Kaiserstraße 12, 76128 Karlsruhe, Germany
wang@ifh.uka.de

Jochen Fröhlich

Institute for Fluid Mechanics, Technical University of Dresden,
George-Bähr Straße, 01062 Dresden, Germany
jochen.froehlich@tu-dresden.de

Vittorio Michelassi

Nuovo Pignone, Via Felipe Matteucci 2, 50127 Florence, Italy
vittorio.michelassi@np.ge.com

Wolfgang Rodi

Institute for Hydromechanics, University of Karlsruhe
Kaiserstraße 12, 76128 Karlsruhe, Germany
rodi@ifh.uka.de

ABSTRACT

Three cases of variable-density turbulent round jets discharging from a straight circular pipe into a weakly confined low-speed co-flowing air stream are studied with the aid of large eddy simulation. The density ratios considered are 0.14 [He/air], 1.0 [air/air] and 1.5 [CO₂/air], with Reynolds numbers of 7000, 21000 and 32000, respectively. Detailed comparisons of the statistics show good agreement with the corresponding experiments. They confirm that a lower-density jet develops more rapidly than a denser jet with the same exit momentum flux. The coherent structures of the three jets are investigated by visualization of the iso-surface of pressure fluctuations and vorticity. In the developing stage of the Kelvin-Helmholtz instability, large finger-shape regions of vorticity are observed for the helium jet close to the nozzle lip. This feature is not found in the air and the CO₂ jet. The occurrence of strong streamwise vorticities across the shear layer in the helium jet is demonstrated by a characteristic variable related to the orientation of the vorticity.

INTRODUCTION

Turbulent flows with variable density, which may be due to temperature variations stemming from reactions or variations in the composition by fluids of different density, exist widely in nature as well as in technical devices. The ability to predict the turbulent mixing in flows with variable density is vital for the modelling of the dynamics of such flows and a prerequisite for predicting turbulent combustion situations. Unlike the extensively studied turbulent flows

with constant density, turbulent flows with variable density are less well understood. Relatively few experimental studies were reported on variable-density turbulent flow situations and especially for flows with large density differences. An experiment with helium/air mixture discharging into a confined swirling flow was carried out by Ahmed et al. (1985). Panchapakesan and Lumley (1993) conducted an experiment with helium injected into open quiescent air from a round nozzle. Later, Djeridane et al. (1996) and Amielh et al. (1996) performed experimental studies of variable-density turbulent jets, including helium, air and CO₂ jets exiting into a low-speed air co-flow. Numerical investigations of this type of flow are also relatively scarce. Jester-Zürker et al. (2005) performed a numerical study of turbulent non-reactive combustor flow under constant and variable-density conditions using a Reynolds-stress turbulence model. They obtained good agreement between simulation and experiment for the constant-density flow, whereas the results for the variable-density flow were less satisfactory. Some large-eddy simulation (LES) of variable density round jets were also performed recently (Zhou et al., 2001, Tyliczszak and Boguslawski, 2006). To the authors' knowledge, however, detailed comparisons of LES results and experimental data for round jets, covering density ratios both lower and larger than unity, are not available in the literature.

The aim of the present work is to perform a detailed comparison of LES results and experimental data for three round jets with density ratios 0.14, 1, and 1.52 respectively, to gain a deeper understanding of the effect of density differences on the jet development.

NUMERICAL METHOD

In this study, the so-called low-Mach number version of the compressible Navier-Stokes equations is employed. With this approach, the pressure P is decomposed into a spatially constant component $P^{(0)}$, interpreted as the thermodynamic pressure, and a variable component $P^{(1)}$, interpreted as the dynamic pressure. $P^{(0)}$ is connected to temperature and density, while $P^{(1)}$ is related to the velocity field only and does not influence the density. Due to this decomposition, sonic waves are eliminated from the flow, so that the time step is not restricted by the speed of sound.

Applying large eddy filtering to the low-Mach number equations, the corresponding filtered LES equations are obtained. The unclosed terms in these equations have to be determined by a subgrid scale (SGS) model. The variable-density dynamic Smagorinsky model by Moin et al. (1991) is used to determine the SGS eddy viscosity, μ_T , in the momentum equations. The SGS scalar flux is modeled by the gradient diffusion model:

$$\overline{\rho \cdot \phi \cdot u_j} - \bar{\rho} \cdot \tilde{\phi} \cdot \tilde{u}_j = - \frac{\mu_T}{Sc_{T,SGS}} \cdot \frac{\partial \tilde{\phi}}{\partial x_j} \quad (1)$$

where $Sc_{T,SGS}$ is the subgrid-scale Schmidt number. $Sc_{T,SGS}$ may be determined with a dynamic procedure, as used for the SGS eddy viscosity (Moin et al., 1991). In this work it is set to $Sc_{T,SGS} = 0.7$.

The simulations were performed with the in-house Finite Volume code LESOCC2C, which is a compressible version of LESOCC2 (Hinterberger, 2004). LESOCC2C is highly vectorized, and parallelization is accomplished by domain decomposition and explicit message passing via MPI. It solves the low-Mach number version of the compressible N-S equations on body-fitted curvilinear block-structured grids. It adopts second-order central schemes for the spatial discretization and a 3-step Runge-Kutta method for the temporal discretization. The convection term of the species equation was discretized with the HLP scheme (Hinterberger, 2004).

COMPUTATION SETUP

Three jets issuing into a slow coflow of air are studied with density ratios equal to 0.14 [Helium/air], 1.0 [air/air], and 1.52 [CO₂/air], respectively (see Fig. 1). These cases correspond to situations studied experimentally by Djeridane et al. (1996) and Amielh et al. (1996). The parameters employed are listed in Table 1, in which the Reynolds number is based on the centre velocity at the jet exit and the jet nozzle diameter. The subscripts 'j' and 'e' represent jet flow and external co-flow, respectively. It is worth noting that the momentum flux is the same for the three cases, $M_j = 0.1N$. The reason for the choice of these cases is that in the flow region investigated inertial forces dominate (Djeridane et al., 1996 and Amielh et al. 1996). The averaging time is given in units of D_j/U_j . Additional averaging was performed in azimuthal direction. Note that this is not effective near the axis so that the quality of averaging is better remote from the axis.

Figure 1 shows a sketch of the flow configuration and the computation domain. The jet discharges from a long pipe into a coflow confined by an outer pipe. The ratio of the pipe diameters, D_e/D_j is 11, so that the confinement is

Table 1: Parameters of the three jets simulated.

Jet	ρ_j/ρ_e	U_j (m/s)	U_e (m/s)	Re_j	t_{aver}
Helium	0.14	32	0.9	7000	1285
Air	1.0	12	0.9	21 000	803
CO ₂	1.52	10	0.9	32 000	1078

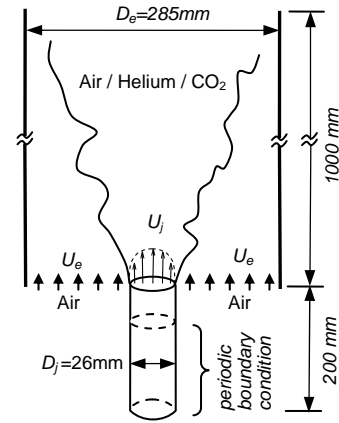


Fig. 1: Sketch of the computational domain.

weak. The computational grid consists of 8 million cells, divided into 251 blocks. To perform a grid resolution study, a coarser grid consisting of 1 million cells was also employed. The grid cells are stretched locally to reduce the cell size near the jet nozzle and across the shear layer. This resulted in a radial extent in wall units along the inner pipe wall of $\Delta r^+ = 3.0, 8.0,$ and 10.5 for the helium, the air and the CO₂ jet, respectively.

A convective outflow boundary condition is imposed at the exit, and a uniform velocity profile without fluctuations at the inlet of the coflow. In order to obtain a fully developed turbulent pipe flow upstream of the jet exit, as indicated by the experimental data, a separate simulation of turbulent pipe flow with streamwise periodic conditions is performed simultaneously (see Fig. 1). The Werner-Wengle wall function (Werner and Wengle, 1993) is used at the pipe walls.

COMPARISON OF STATISTICAL VALUES

Profiles along the jet axis

A comparison of the axial evolution of mean streamwise velocity U_c and mass fraction C_c along the jet axis is shown in Figures 2 and 3, respectively. Analytical curves calculated from the similarity laws proposed for variable-density jets by Chen and Rodi (1980) are also included. The influence of the density difference is obvious: the centerline velocity and concentration of the helium jet decays much faster than in the air and the CO₂ jet. Light gas, helium, tends to mix more rapidly with the ambient air than the heavier gases do (recall that the momentum flux is the same for all flows). This faster mixing of helium is accompanied by a faster increase of turbulence intensity in the near-

nozzle region (see Fig. 4). The potential core of the helium jet is only 3 diameters long, much shorter than that of the air and CO₂ jet. Very good agreement between the LES results and the experimental data is obtained for the helium jet. For the heavier jets, some differences in the U_c decay are observed. They might be due to a small mismatch of inflow conditions.

The influence of the density ratio ρ_j/ρ_e on the decay of U_c and C_c is also described quite well by the similarity laws, but no perfect agreement between the LES and these laws should be expected because the laws are only approximate, and in fact 'x' in the laws should be replaced by the distance from the virtual origin of the jet as a point source.

To show the influence of grid resolution, the results for the helium jet, obtained with the coarse grid, are also shown in Figure 2 and Figure 4.

The evolution of the streamwise velocity rms-fluctuations u' along the jet axis is shown in Figure 4. The influence of the density difference is obvious again: the helium jet decelerates much faster than the two heavier jets. At $x/D_j = 4.5$, the peak value of 17% for u'/U_j is already reached in the helium jet, whereas the peaks for the two heavier gases are lower, less pronounced, and attained further downstream. The fast increase of u'/U_j in the potential core region is due to the growth of the Kelvin-Helmholtz instability across the shear layer. Although the values of u'/U_j for the three jets at positions further downstream, for instance $x/D_j > 25$, are quite different, the values of $u'/(U_c - U_e)$, i.e. u' normalized with the local streamwise velocity difference, are close to each other, at a level about 25-30%.

Figure 5 shows the axial evolutions of the mean mass fraction half-width L_c , as well as the velocity half-width L_u . L_u is defined as the radius at which $U - U_e = 0.5(U_c - U_e)$, in order to take into account the coflow effect. After $x/D_j = 10$, both LES results and experimental results show that: 1) the half-width increases approximately linearly; 2) L_c is always larger than L_u . The former hints to the existence of a similarity behavior, and the latter indicates that the scalar field always spreads faster than the velocity field. It is worth pointing out that, for the helium jet, the downstream values of L_u and L_c are very sensitive, because the profiles are very flat. According to Chen and Rodi (1980), the mean turbulent Schmidt number, Sc_T , is closely related to the square of the ratio L_u/L_c in the similarity region, and a value of $Sc_T = 0.7$ is recommended for round jets. The results in Figure 5 support this value.

Radial distributions

The radial profiles of the normalized mean streamwise velocity U/U_j are shown in Figure 6 for the helium and the CO₂ jet. The results of the air jet are close to those of the CO₂ jet. Very good agreement between LES and experiment is obtained for the helium jet. Starting from the typical turbulent pipe flow profile at $x/D_j = 0.2$, the centerline velocity of the jet decreases faster than for the CO₂ jet, as seen already from Figure 2.

At the first station ($x/D_j = 0.2$ — arrow in Fig. 6b), there is some disagreement for the CO₂ jet. A reason may be that for this case the pipe flow was not fully developed at the exit in the experiment. Beyond $x/D_j = 0.2$, the agreement between LES and experiment is good also for the CO₂ jet.

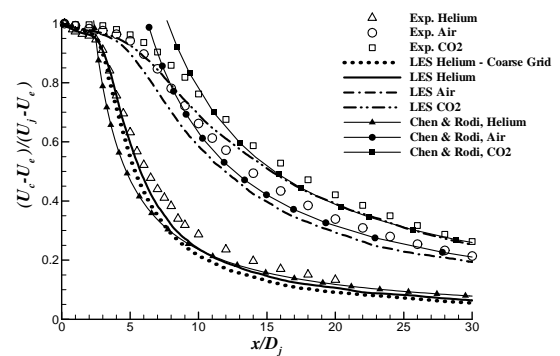


Fig. 2. Mean streamwise velocity along the jet axis. The similarity law proposed by Chen and Rodi (1980) is:

$$U_c/U_j = 6.3(\rho_j/\rho_e)^{1/2}(D_j/x)$$

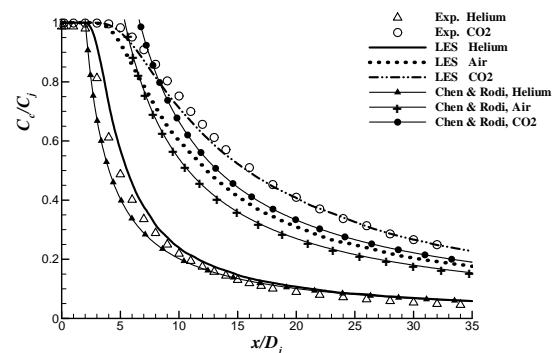


Fig. 3. Mean mass fraction along the jet axis. The similarity law proposed by Chen and Rodi (1980) is:

$$C_c/C_j = 5.4(\rho_j/\rho_e)^{1/2}(D_j/x)$$

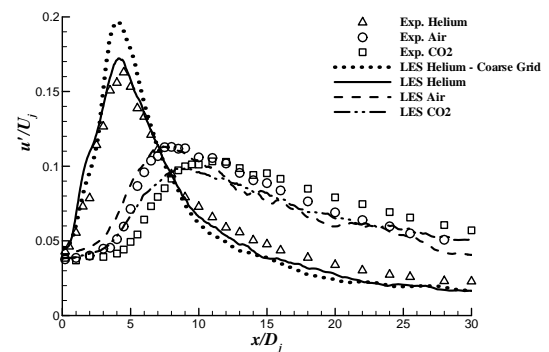


Fig. 4. Streamwise rms-fluctuations along the jet axis.

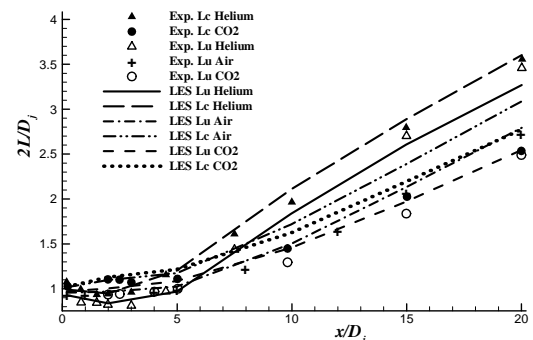


Fig. 5. Half-width of mean mass fraction and half-width of mean streamwise velocity along the jet axis.

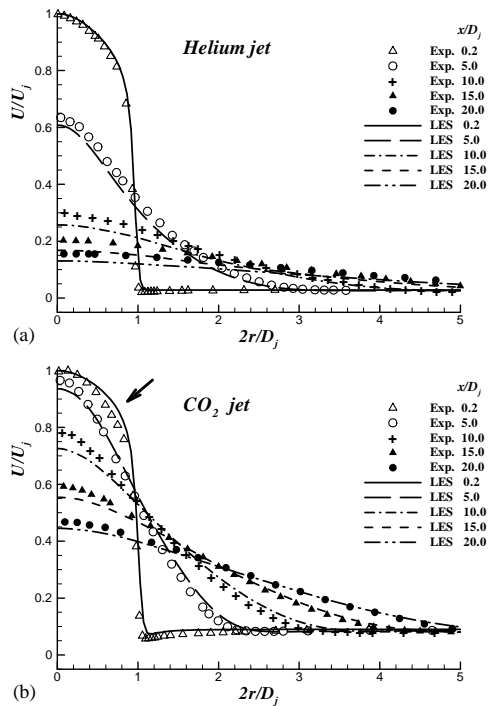


Figure 6. Radial profiles of mean streamwise velocity at several axial positions.

The radial profiles of the streamwise rms-fluctuations at several downstream positions are plotted in Figure 7. Here, the local velocity half-width L_u is used for normalizing the radial coordinates, as in the experimental paper. Again, very good agreement is obtained for the helium jet. At the location very close to the jet nozzle, $x/D_j=0.2$, both jets show a peak value of 0.16 in the shear layer and a value of 0.04 on the axis. Further downstream, the peak of the u' profiles moves to the center and the value of u' on the axis increases due to mixing processes. Finally, the profiles reach an approximate self-similar shape. Figure 7 shows that this transition is much faster for the helium jet than for the CO_2 jet.

Radial distributions of the normalized Reynolds shear stress $\langle u'v' \rangle / U_j U_j$ are plotted in Figure 8. With the two jets, different scales are used for the vertical axes for clarity. The agreement for the helium jet is excellent. In Figure 8a, the peak of $\langle u'v' \rangle / U_j U_j$ at the first section $x/D_j=0.2$ is only 0.003. Further downstream at $x/D_j=2.0$, the maximum is almost four times as large and the shape of the curve is substantially smoother. At even larger x/D_j , the shear stress decays again due to the broadening of the jet and the resulting reduction of gradients. The results for the CO_2 jet in Figure 8b show a substantially stronger peak in the shear stress right at the outlet which is extremely difficult to capture. At $x/D_j=2.0$ and 5.0, the computed profiles have the correct shape but exceed the experimental data by about 25%. Further downstream, the agreement is very good. The reasons for the differences observed may reside in an under-resolution of the very first stages of the initial development or the neglect of any turbulence in the incoming co-flow.

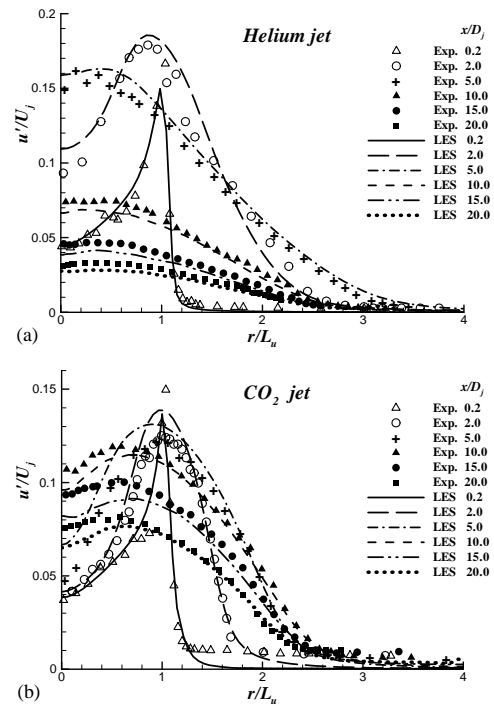


Figure 7. Radial profiles of streamwise rms-fluctuations.

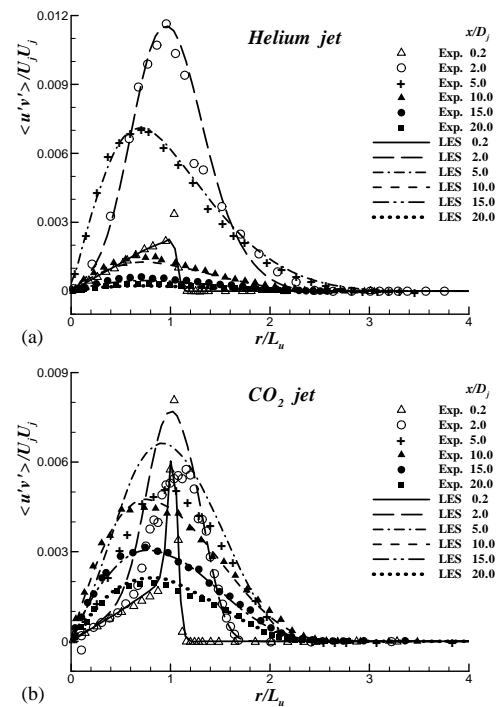


Figure 8. Radial profiles of Reynolds stress.

Pseudo-similarity

Self-similarity can be found in many turbulent flows, of which the constant-density jet is one example. In variable-density turbulent jets, approximate self-similarity exists in some regions, as discussed by Chen and Rodi (1980), so that the term pseudo-similarity is used here. One of these regions is the near field, where buoyancy forces are

negligible compared to inertial forces. The current results mainly pertain to this region so that pseudo-similarity can be expected.

Radial profiles of the mean streamwise velocity and the mean scalar concentration normalized by the values at the jet axis at several streamwise positions are shown in Figure 9. For each curve, the reference length is the local half-width of the respective quantity. The computed and measured profiles collapse fairly well on single curves which are well represented by a Gaussian function, except for the mean scalar fraction at the positions far downstream near the outer edge ($r/L_c > 1.4$). This is due to the confinement starting to have an effect (Djeridane et al. 1996). The good collapse of the radial profiles and the approximately linear increase of the half-width (Fig. 5) demonstrate the pseudo-similarity behavior in the present variable-density jets.

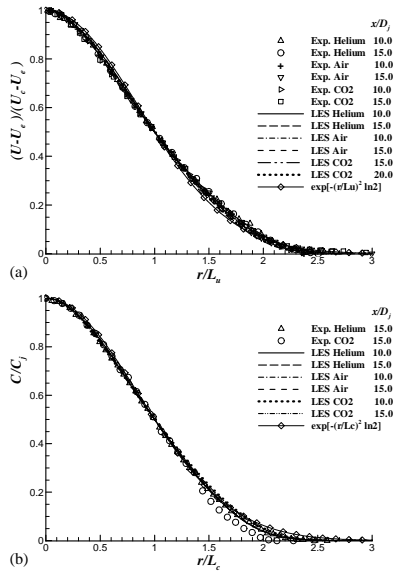


Fig. 9: Similarity profiles of mean velocity and mean mass fraction.

COHERENT STRUCTURES

Gharbi et al. (1995) performed a statistical analysis of the jets considered here. They concluded that the structure of turbulence downstream and in the outer region is similar in all cases while in the near field the properties strongly depend on the density ratio. The present LES data allow to investigate the formation and evolution of coherent structures, which are responsible for the large-scale exchange of mass and momentum. Isosurfaces of the pressure fluctuation p' are employed for this purpose, as successfully used already with swirling constant-density jets by García-Villalba et al. (2006). As in this reference, a 3D box filter is used to smooth p' in a post-processing step in order to enhance the clarity of the picture.

Figure 10 shows such instantaneous iso-surfaces for the helium, air and CO₂ jet, respectively. Shortly downstream of the nozzle, vortex rings are observed in all the three jets due to the Kelvin-Helmholtz instability. Further downstream in the air jet, larger structures form at the outer edge of the jet. In the CO₂ jet, the behaviour is similar, but the distance

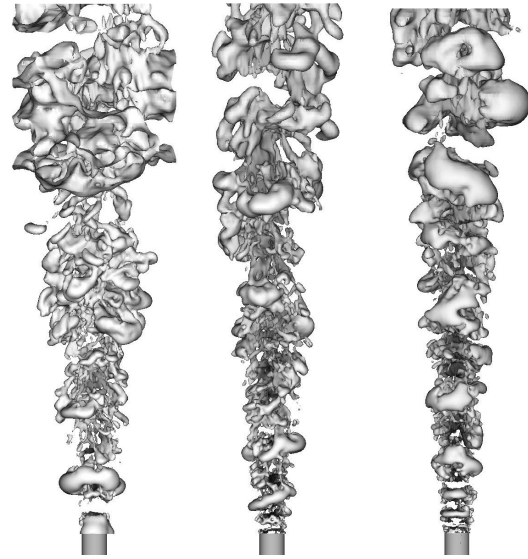


Fig. 10. Iso-surfaces of pressure fluctuations for the helium, air and CO₂ jets, respectively (from left to right).

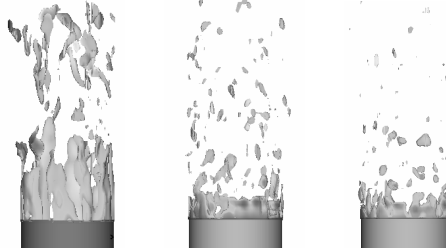


Fig. 11. Iso-surfaces of vorticity for the helium, air and CO₂ jets, respectively (from left to right).

between the vortex rings appears to be shorter and the intermittency lower. For the helium jet in contrast, the outer vortex rings seem to have a larger distance. These observations are made in the near-field region where an inner core and a surrounding flow can be distinguished. In Fig. 10 this would be up to $x/D \approx 10, 14, 18$ for the helium, air, and CO₂ jet, respectively (lighter jets develop faster as discussed above). Beyond this region, the turbulence seems to be fairly homogeneous and vortex rings can no longer be discerned. Figure 11 is concerned with the close vicinity of the jet outlet. It shows iso-surfaces of the vorticity modulus for the three jets in this region. In the helium jet, large vortices are found which are regularly arranged along the lip. The length of these fingers is about one diameter. On the contrary, in the air and the CO₂ jet, only fairly continuous vortex sheets can be seen at the lip of the nozzle, the length of which is shorter. This difference is generated by the Rayleigh-Taylor instability. This secondary instability developing in variable density flows has been studied extensively (Schowalter et al., 1994, Reinaud et al., 1999). Schowalter et al. (1994) show that spanwise vortices generate streamwise vorticity if in a stratified shear layer a lighter fluid drives the heavier fluid.

Relevant for the break up of vortex rings is the generation of streamwise vorticity. Here it is proposed to consider the quantity

$$\Omega_{x/yz} = |\omega_x| / \sqrt{\omega_y^2 + \omega_z^2} \quad (2)$$

measuring the orientation of vorticity with respect to the jet axis. Fig. 12 shows the mean of this quantity. The faster development of the lighter jet and the broader region of axial vorticity in the helium jet is visible. With the helium jet, the outer changeover towards the free stream is somewhat broader. Further investigations of the statistics of the coherent structures are under way.

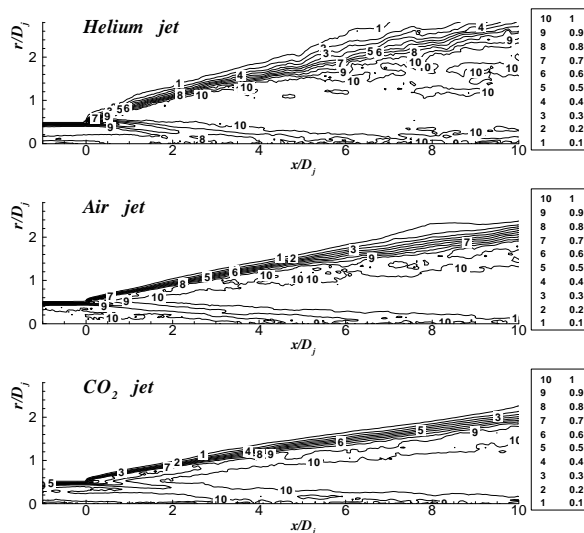


Fig. 12. $\langle \Omega_{x/yz} \rangle$ contours for the helium, air and CO_2 jet, respectively (from top to bottom).

CONCLUSIONS

Three weakly confined turbulent variable-density axisymmetric jets have been studied by LES. The density ratios range from 0.14 to 1.52. A detailed comparison has been made for many statistical quantities, such as the axial evolution of mean streamwise velocity, turbulent intensities, as well as radial profiles of Reynolds stress. The agreement between simulation and experiment is generally very good. For the CO_2 jet the initial stages deviate somewhat but the downstream evolution is again well captured. Additionally, the effect of the density difference on the coherent structures in these jets is also investigated. It is found that some long-finger shaped streamwise vortices, regularly arranged along the jet nozzle lip, are produced in the helium jet, but not in the air and CO_2 jets.

ACKNOWLEDGEMENTS

The authors gratefully acknowledge the support of the German Research Foundation (DFG) through the Collaborative Research Center SFB 606 'Unsteady Combustion'. The computations were performed on the HP-XC clusters of SSK Karlsruhe. F. Anselmet kindly provided the experimental data in electronic form.

REFERENCES

Ahmed, S. A., So, R. M. C., and Mongia, H. C., 1985, "Density Effects on Jet Characteristics in Confined Swirling Flow," *Exp. Fluids*, Vol. 3, pp. 231-238.

Amielh, M., Djeridane, T., Anselmet, F., and Fulachier, L., 1996, "Velocity Near-Filed of Variable Density Turbulent Jets," *Int. J. Heat Mass Transfer*, Vol. 39(10), pp. 2149-2164.

Chen, C. J., and Rodi, W., 1980, "Vertical Turbulent Buoyant Jets—A Review of Experimental Data," *The Science and Application of Heat and Mass Transfer*, Pergamon Press, New York.

Djeridane, T., Amielh, M., Anselmet, F., and Fulachier, L., 1996, "Velocity Turbulence Properties in the Near-Field Region of Axisymmetric Variable Density Jets," *Phys. Fluids*, Vol. 8(6), pp. 1614-1630.

García-Villalba, M., Fröhlich, J., Rodi, W., 2006, "Identification and Analysis of Coherent Structures in the Near Field of a Turbulent Unconfined Annular Swirling Jet Using Large Eddy Simulation", *Phys. Fluids*, Vol. 18, 055103.

Gharbi, A., Amielh, M., and Anselmet, F., 1995, "Experimental Investigation of Turbulence Properties in the Interface Region of Variable Density Jets," *Phys. Fluids*, Vol. 7(10), pp. 2444-2454.

Hinterberger, C., 2004, "Dreidimensionale und Tiefenge-mittelte Large-Eddy-Simulation von Flachwasserströmungen," Ph.D. Thesis, University of Karlsruhe, Germany.

Jester-Zürker, R., Jakirlić, S., and Tropea, C., 2005, "Computational Modelling of Turbulent Mixing in Confined Swirling Environment under Constant and Variable Density Conditions," *Flow, Turbulence and Combustion*, Vol. 75, pp. 217-244.

Moin, P., Squires, K., Cabot, W., and Lee, S., 1991, "A Dynamic Subgrid-Scale Model for Compressible Turbulence and Salar Transport," *Phys. Fluids A*, Vol. 3(11), pp. 2746-2757.

Panchapakesan, N. R., and Lumley, J. L., 1993, "Turbulence Measurements in Axisymmetric Jets of Air and Helium—Part 2. Helium Jet," *J. Fluid Mech.*, Vol. 246, pp. 225-247.

Reinaud, J., Joly, L., Chassaing, P., 1999, "Numerical Simulation of a Variable-Density Mixing-Layer," *Proc., 3rd Int. Workshop on Vortex Flows and Related Numerical Methods*, A. Giovannini et al., ed., ESAIM, Vol. 7, pp. 359-368.

Schwalter, D.G., Van Atta, C.W., and Lasheras, J.C., 1994, "Baroclinic Generation of Streamwise Vorticity in a Stratified Shear Layer," *Meccanica*, Vol. 29, pp. 361-371.

Tyliszczak, A., and Boguslawski, A., 2006, "LES of the Jet in Low Mach Variable Density Conditions," *Direct and Large-Eddy Simulation VI*, Part XII, Springer Netherlands, pp. 575-582.

Werner, H., and Wengle, H., 1993, "Large Eddy Simulation of Turbulent Flow Over and Around a Cube in a Plate Channel," *Proc., 8th Symp. on Turbulent Shear Flows*, Springer Verlag, Berlin.

Zhou, X., Luo, K.H., and Williams, J.J.R., 2001, "Study of Density Effects in Turbulent Buoyant Jets Using Large-Eddy Simulation," *Theor. Comput. Fluid Dyn.*, Vol. 15, pp. 95-120.